

Constraints on $f(T)$ Gravity from Solar Neutrino Conversion

H. Yazdani Ahmadabadi* and H. Mohseni Sadjadi†

Department of Physics, University of Tehran,
P. O. B. 14395-547, Tehran 14399-55961, Iran

February 13, 2026

Abstract

We report new constraints on the parameters of $f(T)$ teleparallel gravity, derived from its imprints on neutrino flavor oscillations. Our analysis reveals that the presence of space-time torsion can alter both vacuum oscillations and the matter-enhanced Mikheyev–Smirnov–Wolfenstein (MSW) resonance. By using data from solar neutrino experiments: Super-Kamiokande, SNO, Borexino, and KamLAND, we perform a combined analysis to place the first direct observational bounds on the neutrino-torsion coupling and $f(T)$ parameters. These results establish neutrino phenomenology as a novel astrophysical probe for testing fundamental modifications of gravity.

1 Introduction

The discovery of neutrino flavor oscillation marked a major breakthrough in particle physics, providing the first direct evidence that neutrinos have mass. Proposed to solve the solar neutrino deficit [1–3], this phenomenon was confirmed by landmark experiments like Super-Kamiokande (SK) [4] and the Sudbury Neutrino Observatory (SNO) [5]. High-precision measurements of neutrino mass and mixing parameters have been achieved using a diverse array of sources, including solar [6–9], atmospheric [10–12], reactor [13, 14], and accelerator [15] neutrinos. The accepted theory is that neutrinos oscillate between three flavors as they travel. When passing through matter (like the Sun), the significant Mikheyev–Smirnov–Wolfenstein (MSW) effect [16, 17] occurs, enhancing this flavor conversion. Consequently, neutrinos are probes of new physics, with fundamental questions about their mass origin and their Dirac or Majorana nature remaining pressing open issues.

Beyond the established phenomenon of neutrino oscillations in flat spacetime, their behavior in curved spacetime has become a significant area of research within extended gravity theories [18–24]. Neutrinos play a crucial role in the early universe, and detecting the cosmic neutrino background (a goal of projects like PTOLEMY [25]) would powerfully test the standard cosmological model. Furthermore, neutrinos with varying masses have been proposed as a candidate to explain dark energy. In these models [26–32], neutrinos and a scalar field are linked by the neutrino mass, which has roots in the dark energy model. The dependence of the neutrino mass on the environment due to the interactions with dark sectors demonstrates that the non-standard interactions between the scalar field and matter components modifies the MSW effect, and subsequently, generates damping signatures which triggers the idea that a second-order effect might contribute to the experimentally confirmed deficit of neutrino flux [28–31].

A promising direction of related research is the teleparallel equivalent of general relativity (TEGR) [33–39]. TEGR represents a geometric reformulation of general relativity that employs an enriched geometric structure, which may offer new mechanisms for explaining cosmological phenomena. Following the observational discovery of the accelerated expansion of the Universe [40, 41], considerable effort has been devoted to extending GR in order to accommodate these observations [42, 43] without resorting to the introduction of dark energy. Within the TEGR framework, gravitation is described by torsion rather than

*hossein.yazdani@ut.ac.ir

†mohsenisad@ut.ac.ir

curvature, and the gravitational action is constructed from the torsion scalar T instead of the Ricci scalar R . This formulation is naturally defined on a Riemann–Cartan spacetime equipped with the Weitzenböck connection [44], which is characterized by vanishing curvature and non-vanishing torsion.

A notable realization of this approach is provided by modified teleparallel gravity in the form of the $f(T)$ theory, particularly the model $f(T) = T + \alpha T^k$ [45–54]. In this class of models, the torsion scalar appearing in the TEGR action is generalized by the inclusion of nonlinear corrections parameterized by the constants α and k , leading to modified gravitational dynamics that can potentially address late-time cosmic acceleration and other deviations from standard general relativity.

Accordingly, the present study aims to advance beyond a heuristic description of neutrino flavor transitions by formulating a theoretical framework based on $f(T)$ gravity. Within this model, we evaluate how spacetime torsion influences oscillation phenomena. We subsequently derive general, analytical expressions that quantify both the phase shift of neutrino oscillations and the modified mixing parameters inside matter. These modifications affect both the fundamental vacuum oscillations and the well-established MSW resonance mechanism, suggesting that torsion may not be neglected in astrophysical environments. These formulae, which constitute the principal result of this work, provide a new tool for probing gravitational effects on quantum-mechanical particles in extreme environments. An advantage of this scenario is the availability of an exact analytical solution to the Dirac equation, which allows for the direct application of the formalism introduced in this work.

This work establishes a direct link between quantum particle phenomenology and the geometric formulation of gravity. It provides a framework for testing $f(T)$ gravity model with current and future neutrino observatories such as JUNO, DUNE, and Hyper-Kamiokande. If torsion effects are detected, they would offer new insights into the nature of dark energy, neutrino mass generation, and the unification of gravity with particle physics.

This paper is structured as follows. In Section 2, we review the theoretical framework of $f(T)$ gravity and solve its field equations for spherically symmetric spacetimes under the “weak-field approximation”, considering the polynomial density profile. Section 3 presents the exact solution to the Dirac equation with a torsion-neutrino coupling term, demonstrating its effects on the phase of the neutrino wavefunction. This section also examines the effects of this new coupling on the neutrino mass and energy terms, which in turn modifies the neutrino Hamiltonian, leading to effective mass and mixing parameters. In Section 4, we present the numerical results, compare them against observational data, and provide the ensuing constraints on the model’s parameters (e.g., α). Concluding remarks are provided in Section 5.

Throughout the paper, we use units $\hbar = c = 1$ and metric signature $(+, -, -, -)$.

2 $f(T)$ Gravity and Spacetime Torsion

Teleparallel gravity provides an alternative geometric formulation of general relativity, in which the gravitational interaction is described by the spacetime torsion rather than curvature. This framework is based on the Weitzenböck connection, which is characterized by vanishing curvature and non-zero torsion, in contrast to the Levi-Civita connection of GR that is torsion-free but curved [33–37]. Within this formulation, gravitational effects arise entirely from torsional degrees of freedom, while spacetime curvature plays no dynamical role.

The fundamental dynamical variables in teleparallel gravity are the tetrad fields $e_{\hat{\mu}}^{\hat{a}}$, which define an orthonormal basis on the tangent space at each spacetime point [55]. The corresponding spacetime metric $g_{\mu\nu}$ is constructed from the tetrads according to

$$g_{\mu\nu} = e_{\hat{\mu}}^{\hat{a}} e_{\hat{\nu}}^{\hat{b}} \eta_{\hat{a}\hat{b}}, \quad (1)$$

where Greek indices label spacetime coordinates and Latin indices with a hat correspond to locally inertial Lorentz frames, with $\eta_{\hat{a}\hat{b}} = \text{diag}(+1, -1, -1, -1)$. Within the framework of the TEGR, the Weitzenböck connection is constructed entirely from the tetrad fields and is given by

$$\Gamma^{\lambda}_{\mu\nu} = e_{\hat{a}}^{\lambda} \partial_{\nu} e_{\hat{\mu}}^{\hat{a}}. \quad (2)$$

The associated torsion tensor is defined as

$$\begin{aligned} T^\lambda{}_{\mu\nu} &= \Gamma^\lambda{}_{\nu\mu} - \Gamma^\lambda{}_{\mu\nu} \\ &= e_{\hat{a}}^\lambda (\partial_\mu e_{\hat{\nu}}^{\hat{a}} - \partial_\nu e_{\hat{\mu}}^{\hat{a}}). \end{aligned} \quad (3)$$

The torsion tensor captures the antisymmetric part of the connection and fully encodes the gravitational degrees of freedom in teleparallel gravity.

The dynamics of TEGR are governed by the torsion scalar T , constructed from specific quadratic contractions of the torsion tensor

$$T = \frac{1}{4} T^{\mu\nu\lambda} T_{\mu\nu\lambda} + \frac{1}{2} T^{\mu\nu\lambda} T_{\nu\mu\lambda} - T^\mu T_\mu. \quad (4)$$

This particular combination is chosen such that the torsion scalar differs from the Ricci scalar \mathcal{R} of the Levi–Civita connection by a total divergence [56, 57]

$$\mathcal{R} = -T + 2\nabla_\mu T^\mu, \quad (5)$$

thereby ensuring the dynamical equivalence of TEGR and GR at the level of the field equations.

Under the Lorentz group, the torsion tensor admits an irreducible decomposition into vector, axial, and purely tensorial components [34]. From the torsion tensor, one defines the torsion vector

$$T_\mu = T^\lambda{}_{\lambda\mu}, \quad (6)$$

which corresponds to its trace and might play an important role in the teleparallel action. Furthermore, the axial torsion vector is defined through the dual of the torsion tensor [58]

$$A^\mu = \epsilon^{\alpha\beta\gamma\mu} T_{\alpha\beta\gamma}. \quad (7)$$

This quantity represents the totally antisymmetric part of the torsion tensor and is particularly relevant in theories with fermionic matter, where it naturally couples to axial currents. Here, $\epsilon^{\alpha\beta\gamma\mu}$ denotes the contravariant Levi–Civita tensor, which enables the dualization of antisymmetric tensors in curved spacetime. It is related to the Levi–Civita symbol $\delta^{\alpha\beta\gamma\mu}$ —a tensor density of weight +1 with $\delta^{0123} = +1$ —via the determinant of the metric g , i.e., we have

$$\epsilon^{\alpha\beta\gamma\mu} = \frac{\delta^{\alpha\beta\gamma\mu}}{\sqrt{-g}}, \quad (8)$$

which guarantees that $\epsilon^{\alpha\beta\gamma\mu}$ transforms as a genuine tensor under general coordinate transformations [58].

A widely studied extension of TEGR is obtained by replacing the torsion scalar T with a general function $f(T)$, in close analogy to $f(R)$ gravity [59, 60]. The action for $f(T)$ gravity is given by

$$\mathcal{S} = \frac{M_p^2}{2} \int d^4x [\mathcal{E} f(T)] + \mathcal{S}_m, \quad (9)$$

where $M_p = 1/\sqrt{8\pi G}$ is the reduced Planck mass, $\mathcal{E} = \sqrt{-\det(g_{\mu\nu})}$ denotes the determinant of the tetrad, and \mathcal{S}_m represents the action of the matter fields. In contrast to $f(R)$ theories, the field equations of $f(T)$ gravity remain of second order due to the absence of higher-derivative terms in the torsion scalar.

We start from the metric [52]

$$ds^2 = e^{A(r)} dt^2 - e^{B(r)} dr^2 - r^2 d\Omega^2, \quad (10)$$

looking for spherically symmetric solutions of the field equations, where $d\Omega^2 = d\theta^2 + \sin^2\theta d\phi^2$. The simplest tetrad yielding the above metric is the diagonal one; however, it does not properly parallelize the static spherically symmetric geometry in the context of $f(T)$ gravity [52, 61]. So, we will work with a specific tetrad, i.e., the “good” tetrad, of the form

$$e_{\hat{\mu}}^{\hat{a}} = \begin{pmatrix} e^{\frac{A}{2}} & 0 & 0 & 0 \\ 0 & e^{\frac{B}{2}} \sin\theta \cos\phi & -r \cos\theta \cos\phi & r \sin\theta \sin\phi \\ 0 & e^{\frac{B}{2}} \sin\theta \sin\phi & -r \cos\theta \sin\phi & -r \sin\theta \cos\phi \\ 0 & e^{\frac{B}{2}} \cos\theta & r \sin\theta & 0 \end{pmatrix}, \quad (11)$$

that does not yield a constant torsion scalar. This tetrad eliminates inertial contributions and yields a consistent spherically symmetric solution in $f(T)$ gravity [61]. In this geometry, the axial torsion vector vanishes identically, so axial couplings do not contribute. According to this tetrad field, the torsion scalar is explicitly given by

$$T(r) = \frac{2e^{-B(r)}(1 + e^{B(r)/2})}{r^2} \left[1 + e^{B(r)/2} + rA'(r) \right]. \quad (12)$$

Variation of the action with respect to the tetrad $e_{\hat{\alpha}}^{\mu}$ gives the following set of equations [52]:

$$\mathcal{E}^{-1} \partial_{\mu} (\mathcal{E} e_{\hat{\alpha}}^{\rho} S_{\rho}^{\mu\nu}) f_T + e_{\hat{\alpha}}^{\lambda} S_{\rho}^{\nu\mu} T^{\rho}_{\mu\lambda} f_T + e_{\hat{\alpha}}^{\rho} S_{\rho}^{\mu\nu} (\partial_{\mu} T) f_{TT} + \frac{1}{4} e_{\hat{\alpha}}^{\nu} f = 4\pi G e_{\hat{\alpha}}^{\mu} \mathcal{T}_{\mu}^{\nu}, \quad (13)$$

where \mathcal{T}_{μ}^{ν} is the matter energy-momentum tensor and subscript T denotes differentiation with respect to torsion scalar T . In the rest of the paper, we consider $f(T) = T + \alpha T^k$ [52–54], where α is a constant parameter, implying the deviation of such theories from the standard TEGR. Indeed, for actual physical situations such as in the solar system, the gravity is relatively weak compared to the strong-field regimes near black holes or neutron stars. So, we expand the metric exponentials to linear order and write

$$e^{A(r)} \approx 1 + A(r), \quad e^{B(r)} \approx 1 + B(r). \quad (14)$$

This approximation is called the “weak-field limit”. By substituting the tetrads from Eq. (11) into the corresponding field equations and linearizing them with respect to the functions $A(r)$ and $B(r)$, we derive a simplified set of equations

$$r^3 B'(r) + r^2 B(r) + 96\alpha - 8\pi G r^4 \rho = 0, \quad (15)$$

$$r^3 A'(r) + r^2 B(r) - 32\alpha + 4\pi G r^4 p = 0, \quad (16)$$

and

$$r^4 A''(r) - r^3 [A'(r) + B'(r)] + 2r^2 B(r) - 128\alpha = 0, \quad (17)$$

where ρ and p are the energy density and pressure of matter component, and prime denotes differentiation with respect to the radial coordinate r . Throughout the present analysis, we set the power of the second term in the $f(T)$ function to $k = 2$, i.e., we investigate $f(T) = T + \alpha T^2$. The simplified equations are then solved under both vacuum conditions and the polynomial matter density profile, with the resulting solutions shown below.

2.1 Vacuum Solution

In vacuum, i.e., for $\rho = p = 0$, exact solutions of (15)-(17) are given by

$$\begin{aligned} A(r) &= -\frac{32\alpha}{r^2} - \frac{C}{r}, \\ B(r) &= \frac{96\alpha}{r^2} + \frac{C}{r}, \end{aligned} \quad (18)$$

where C is an integration constant. Setting $C = 2GM$ gives the weak-field limit of the Schwarzschild solution plus a correction due to the deviation from TEGR. Therefore, we have

$$ds^2 = \left(1 - \frac{2GM}{r} - \frac{32\alpha}{r^2} \right) dt^2 - \left(1 + \frac{2GM}{r} + \frac{96\alpha}{r^2} \right) dr^2 - r^2 d\Omega^2. \quad (19)$$

Plugging the components (18) into the general expression for the tetrad (11), we find the torsion scalar

$$T(r) = \frac{8}{r^2} - \frac{128\alpha}{r^4}, \quad (20)$$

where the last term is due to the higher-order torsion ($\propto T^2$) effects.

Confining neutrino propagation to the equatorial plane by setting $\theta = \pi/2$ and $\phi = 0$ simplifies the radial distance to $x = r$. This simplification means that T_1 below depends solely on the radial coordinate, which will facilitate the derivation of subsequent relations. Thus, the only non-zero component of the torsion vector is obtained as

$$\begin{aligned} T_1(r) &\equiv T^\lambda{}_{\lambda 1} \\ &= -\frac{4}{r} - \frac{3GM}{r^2} - \frac{128\alpha}{r^3}. \end{aligned} \quad (21)$$

2.2 Solution inside Matter

We consider a static, spherically symmetric distribution of non-relativistic matter with radial density profile $\rho(r)$. Throughout this analysis, pressure contributions to the gravitational field are neglected, which constitutes a valid approximation in the weak-field regime. Although realistic models of the solar interior rely on detailed helioseismic observations and sophisticated numerical simulations grounded in stellar structure theory [62], it is often useful to adopt simplified analytic density profiles for theoretical investigations [63]. One such analytically tractable approximation for the solar density distribution is given by a polynomial model of the form

$$\rho(r) = \begin{cases} \rho_0 \left(a \left(\frac{r}{R_\odot} \right)^4 + b \left(\frac{r}{R_\odot} \right)^3 + c \left(\frac{r}{R_\odot} \right)^2 + d \left(\frac{r}{R_\odot} \right) + e \right) & (\text{for } r \leq R_\odot), \\ 0 & (\text{for } r > R_\odot) \end{cases}, \quad (22)$$

where a , b , c , d , and e are dimensionless fitting parameters [63], ρ_0 sets the overall density scale, and R_\odot denotes the solar radius. Introducing the dimensionless radial coordinate $R = r/R_\odot$, the interior of the Sun corresponds to the interval $R \in [0, 1]$. Solving the modified gravitational field equations (15)-(17) for this density profile yields the metric functions

$$\begin{aligned} A(R) &= -\frac{32\alpha}{R^2 R_\odot^2} - \frac{2GM}{RR_\odot} + 2\pi G\rho_0 R_\odot^2 \left(\frac{2}{21}aR^6 - \frac{2}{15}bR^5 + \frac{1}{5}cR^4 - \frac{1}{3}dR^3 \right), \\ B(R) &= \frac{96\alpha}{R^2 R_\odot^2} + \frac{2GM}{RR_\odot} + 2\pi G\rho_0 R_\odot^2 \left(\frac{4}{7}aR^6 - \frac{2}{3}bR^5 + \frac{4}{5}cR^4 - dR^3 + \frac{4}{3}eR^2 \right). \end{aligned} \quad (23)$$

These expressions show that, in the weak-field regime, the Schwarzschild solution is modified by additional terms proportional to the $f(T)$ parameter α . In the vacuum limit, obtained by taking $\rho_0 \rightarrow 0$, the matter-dependent contributions vanish and the solution reduces to the vacuum case given in Eq.(18). Furthermore, an examination of the α -dependent corrections reveals that they decay at large radial distances. Consequently, the metric asymptotically approaches the Schwarzschild solution at large distances from the spherical source.

After straightforward calculations, the corresponding metric is explicitly given by

$$\begin{aligned} ds^2 &= \left(1 - \frac{2GM}{RR_\odot} - \frac{32\alpha}{R^2 R_\odot^2} + 2\pi G\rho_0 R_\odot^2 \left(\frac{2a}{21}R^6 - \frac{2b}{15}R^5 + \frac{c}{5}R^4 - \frac{d}{3}R^3 \right) \right) dt^2 \\ &\quad - \left(1 + \frac{2GM}{RR_\odot} + \frac{96\alpha}{R^2 R_\odot^2} + 2\pi G\rho_0 R_\odot^2 \left(\frac{4a}{7}R^6 - \frac{2b}{3}R^5 + \frac{4c}{5}R^4 - dR^3 + \frac{4e}{3}R^2 \right) \right) R_\odot^2 dR^2 - R_\odot^2 R^2 d\Omega^2. \end{aligned} \quad (24)$$

The terms proportional to α represent higher-order torsion contributions to the function $f(T)$. The polynomial constants modify both the timelike and radial components of the metric in a radius-dependent manner. From these metric solutions, we can derive important geometrical quantities. As a consequence, the above results can be applied to obtain the torsion scalar

$$T(R) = \frac{8}{R^2 R_\odot^2} - \frac{128\alpha}{R^4 R_\odot^4} - \frac{32}{3}\pi G\rho_0 e. \quad (25)$$

Remarkably, except for a constant shift proportional to the parameter e , this expression is independent of the detailed matter density profile $\rho(r)$, depending explicitly only on the torsion parameter α . This indicates

that, in this case, torsion effects are dominated by the purely geometric T^2 contributions, while the coupling to matter, only through the global constant term $\rho_0 e$, plays only a subleading and non-dynamical role. Furthermore, the non-zero component of the torsion vector takes a more complicated form

$$T_1(R) = -\frac{4}{RR_\odot} - \frac{3GM}{R^2 R_\odot^2} - \frac{128\alpha}{R^3 R_\odot^3} - \pi G \rho_0 R_\odot \left(\frac{12}{7} a R^5 - 2b R^4 + \frac{12}{5} c R^3 - 3d R^2 \right). \quad (26)$$

For the above solutions to remain physical, α must be small enough that the metric components do not exhibit unphysical singularities or sign changes outside the horizon. Solar system tests [64–68] can place bounds on α . In the present work, however, we try to put bounds on this parameter using the neutrino oscillation observations [69].

3 Torsion Effects on Neutrino Oscillations

This study investigates how spacetime torsion modifies neutrino flavor oscillations within teleparallel gravity, an alternative geometric formulation in which gravitation is mediated by torsion rather than curvature. Within the standard prescription, the torsion tensor $T^\rho{}_{\mu\nu}$ can be decomposed into three irreducible components: a vector part $T_\mu = T^\nu{}_{\nu\mu}$ (see Eq.(6)), an axial-vector part $A^\mu = \frac{1}{6}\epsilon^{\mu\nu\rho\sigma}T_{\nu\rho\sigma}$ (see Eq.(7)), and a purely tensorial part $t_{\lambda\mu\nu}$ [34, 70, 71]. This decomposition leads to an effective torsion-induced vector and axial-vector coupling Lagrangian, i.e., we have $\mathcal{L}^{\text{VA}} \propto \kappa^V T_\mu \bar{\psi} \gamma^\mu \psi + \kappa^A A_\mu \bar{\psi} \gamma^\mu \gamma^5 \psi$, where κ 's denote the neutrino-torsion part coupling coefficients.

For Dirac neutrinos, the non-vanishing vector current $\bar{\nu}_D \gamma^\mu \nu_D$ yields a coupling to T_μ , leading to a modified Dirac equation of the form $(i\gamma^\mu D_\mu - m + \kappa^V \gamma^\mu T_\mu) \nu_D = 0$, which effectively describes propagation in an external vector potential. In contrast, for Majorana neutrinos, the vector current $\bar{\nu}_M \gamma^\mu \nu_M$ identically vanishes [72].

Any possible coupling of Majorana neutrinos with torsion might arise through the axial-vector current $\bar{\nu}_M \gamma^\mu \gamma^5 \nu_M$, coupled to A_μ . In the simplest spherically symmetric teleparallel geometries—e.g., TEGR with a good tetrad (11)—the axial-vector component vanishes, $A^\mu = 0$ [73], while T_μ remains non-zero. Moreover, the covariant derivative $D_\mu = \partial_\mu + \Gamma_\mu$ in the Dirac equation contains the spin connection Γ_μ , defined as $\Gamma_\mu = \frac{1}{8}[\gamma^{\hat{a}}, \gamma^{\hat{b}}] e_{\hat{a}}^\nu e_{\hat{b}\nu;\mu}$ to ensure local Lorentz covariance. A relevant term is the contraction $\gamma^{\hat{a}} e_{\hat{a}}^\mu \Gamma_\mu$, which can be shown [18, 24] in details as

$$\gamma^{\hat{a}} e_{\hat{a}}^\mu \Gamma_\mu = \gamma^{\hat{a}} e_{\hat{a}}^\mu \left[i A_\mu \left(-(-g)^{-\frac{1}{2}} \frac{\gamma_5}{2} \right) \right], \quad (27)$$

where g denotes again the metric determinant and γ_5 is the chiral gamma matrix. As mentioned earlier, since $A^\mu = 0$ under spherical symmetry, this term does not contribute.

In the spherically symmetric geometry considered here, the axial torsion A^μ vanishes for the chosen tetrad leaving only the vector coupling term. For Majorana neutrinos, the vector current vanishes identically, so we restrict our analysis to Dirac neutrinos in what follows.

Following the above considerations, we model torsion effects from an astrophysical source through a vector field T_μ . The neutrino propagation is then described by the action

$$\begin{aligned} \mathcal{S}_\nu = \int d^4x e \left[- \sum_{\alpha,\beta} \nu_{\alpha L}^\dagger m_{\alpha\beta} \nu_{\beta R} - \sum_{\alpha,\beta} \nu_{\alpha R}^\dagger m_{\beta\alpha}^* \nu_{\beta L} \right. \\ \left. + i \sum_{\alpha} \left(\nu_{\alpha L}^\dagger \sigma_L^\mu D_\mu \nu_{\alpha L} + \nu_{\alpha R}^\dagger \sigma_R^\mu D_\mu \nu_{\alpha R} \right) \right. \\ \left. + \sum_{\alpha} \kappa T_\mu \left(\nu_{\alpha L}^\dagger \sigma_L^\mu \nu_{\alpha L} + \nu_{\alpha R}^\dagger \sigma_R^\mu \nu_{\alpha R} \right) \right]. \quad (28) \end{aligned}$$

The mass terms are defined by the components $m_{\alpha\beta}$ of a 3×3 flavor-basis matrix acting on the left- and right-handed two-component spinors, $\nu_{\alpha(L,R)}$. The chiral structure is encoded in the right- and left-handed Pauli matrices, $\sigma_R^\mu = (\sigma^0, \sigma^1, \sigma^2, \sigma^3)$ and $\sigma_L^\mu = (\sigma^0, -\sigma^1, -\sigma^2, -\sigma^3)$, respectively. Furthermore, the Lorentz vector field for spinors is expressed as $\bar{\psi} \gamma^\mu \psi = \psi_L^\dagger \sigma_L^\mu \psi_L + \psi_R^\dagger \sigma_R^\mu \psi_R$ [74], as reflected in the action's third line. Also, the superscript V on the coupling constant κ has been dropped for simplicity.

3.1 Vacuum Neutrino Oscillation

Neutrino flavor oscillation is a process when a neutrino is created with a particular flavor in the source and then travels a relatively long distance and finally contributes to weak interactions in the detectors to show a neutrino with a different flavor. This phenomenon has led to a change in our belief in the mass of neutrinos. We can write each flavor eigenstate as a mixing of three mass eigenstates, which is given by

$$\nu_{\alpha(L,R)} = \sum_i U_{\alpha i}^{*(L,R)} \nu_{i(L,R)}, \quad (29)$$

where $U_{\alpha i}$'s are components of the Pontecorvo-Maki-Nakagawa-Sakata (PMNS) unitary mixing matrix, written as

$$U = \begin{pmatrix} c_{12}c_{13} & s_{12}c_{13} & s_{13}e^{-i\delta} \\ -s_{12}c_{23} - c_{12}s_{23}s_{13}e^{i\delta} & c_{12}c_{23} - s_{12}s_{23}s_{13}e^{i\delta} & s_{23}c_{13} \\ s_{12}s_{23} - c_{12}c_{23}s_{13}e^{i\delta} & -c_{12}s_{23} - s_{12}c_{23}s_{13}e^{i\delta} & c_{23}c_{13} \end{pmatrix}, \quad (30)$$

where $c_{ij} \equiv \cos \theta_{ij}$, $s_{ij} \equiv \sin \theta_{ij}$, and δ is the Dirac CP-violating phase.

Massless neutrinos would have plane-wave solutions of negative helicity. However, by introducing the masses for neutrinos, we may redefine its wavefunctions as

$$\begin{aligned} \nu_{\alpha L}(x, t) &= e^{-iE_\nu(t-t_0)} e^{+iE_\nu(x-x_0)} h_\alpha(x) \begin{pmatrix} 0 \\ 1 \end{pmatrix}, \\ \nu_{\alpha R}(x, t) &= e^{-iE_\nu(t-t_0)} e^{+iE_\nu(x-x_0)} g_\alpha(x) \begin{pmatrix} 0 \\ 1 \end{pmatrix}. \end{aligned} \quad (31)$$

By varying the neutrino action (28) with respect to the left- and right-handed spinors, and using relations (31), the equations of motion are given by

$$i \frac{dh_\alpha(x)}{dx} - m_{\alpha\beta} g_\beta(x) + \kappa T_1(x) h_\alpha(x) = 0, \quad (32)$$

and

$$\left[2E_\nu - \kappa T_1(x) - i \frac{d}{dx} \right] g_\alpha(x) - m_{\beta\alpha}^* h_\beta(x) = 0. \quad (33)$$

Since the magnitude of the second term is much lower than the first one in (33) (which includes neutrino energy), we can neglect that (i.e., $|dg_\alpha/dx| \ll 2E_\nu g_\alpha$). Hence, obtaining the function $g_\alpha(x)$ and replacing that in Eq.(32) gives the equation of motion

$$i \frac{dh_i(x)}{dx} - \frac{\hat{m}_i^2}{2\hat{E}_\nu} h_i(x) = 0, \quad (34)$$

where we have used the characteristics $m_{\alpha\beta} = U_{\alpha i}^* U_{\beta i} m_i$ and $h_\alpha(x) = U_{\alpha i}^* h_i(x)$ (based on the mixing relation (29)). Within the framework of $f(T)$ gravity, the presence of spacetime torsion generates additional terms in the equation of motion that couples to the neutrino's spinor field. These terms are mathematically equivalent to a shift in both the neutrino energy and its effective mass-squared, motivating the definition of the effective quantities \hat{E}_ν and \hat{m}_i^2 . Physically, the redefinition of the neutrino energy, i.e.,

$$\hat{E}_\nu \equiv E_\nu - \frac{1}{2} \kappa T_1(x), \quad (35)$$

can be interpreted as an effective potential induced by spacetime torsion. The quantity \hat{E}_ν is an effective energy appearing in the neutrino propagation equation after separating the spinor components. It is not the conserved Killing energy with the timelike Killing vector of the static metric. Instead, its spatial variation encodes the work done by the torsion field on the neutrino as it propagates, analogous to a potential energy term in non-relativistic quantum mechanics. This torsion-induced contribution plays a role analogous to

the matter potential in the MSW effect, but with a fundamentally geometric origin rather than arising from weak interactions with a background medium. The dependence on the component $T_1(x)$ indicates that neutrino propagation becomes sensitive to the local spacetime structure, leading to the position-dependent modifications of the neutrino oscillation phase.

Similarly, the effective mass-squared includes torsion-induced corrections proportional to both the neutrino energy and the coupling parameter, i.e., we have

$$\begin{aligned}\hat{m}_i^2 &\equiv m_i^2 - 2\hat{E}_\nu \kappa^{(i)} T_1(x) \\ &= m_i^2 - 2E_\nu \kappa^{(i)} T_1(x) + \mathcal{O}\left(\kappa^{(i)2} T_1^2(x)\right).\end{aligned}\quad (36)$$

At leading order, this correction introduces an energy-dependent shift to the neutrino mass spectrum, which directly affects the oscillation phase. This energy dependence is particularly noteworthy, as it deviates from the standard vacuum oscillation framework, where masses are constant parameters. Consequently, torsion may produce novel oscillation patterns or phase shifts even in the absence of matter, potentially modifying standard oscillation effects.

Now, we solve the equation (34) easily to obtain the neutrino's wavefunction

$$\mathbf{v}_i(x, t) = e^{-iE_\nu[(t-t_0)-(x-x_0)]} e^{-i\Phi_i(x)} \mathbf{v}_i(x_0, t_0).\quad (37)$$

Therefore, the quantity

$$\Phi_i(x) = \int_{x_0}^x \left[\frac{m_i^2}{2E_\nu - \kappa^{(i)} T_1(x)} - \kappa^{(i)} T_1(x) \right] dx\quad (38)$$

is defined as the modified phase of oscillations in vacuum. This oscillation phase is similar to that flat spacetime (the mass-squared term), but is modified due to the background torsion. The superscript (i) implies various coupling strengths in the mass-basis, showing the torsion effects.

In the specific regime, where the product of the torsion coupling constant and the background torsion field is significantly smaller than the neutrino energy $\kappa T_1(x) \ll E_\nu$, the modification to the standard neutrino oscillation phase can be explicitly calculated. Under this assumption, the phase difference Φ_{ij} between neutrino mass eigenstates is given by

$$\Phi_{ij} = \frac{\Delta m_{ij}^2 (x - x_0)}{2E_\nu} - \Delta \kappa^{(ij)} \int_{x_0}^x T_1(x) dx.\quad (39)$$

Here, $\Delta \kappa^{(ij)} = \kappa_i - \kappa_j$ represents the difference in how each mass eigenstate couples to the spacetime torsion field. This formulation demonstrates that the oscillation phase acquires a novel contribution from the integral of the torsion field along the neutrino's path, in addition to the conventional phase-term dependent on the squared mass difference Δm_{ij}^2 .

Another situation arises if the torsion coupling κ is universal, i.e., ($\kappa_i = \kappa_j$). In this case, the coupling difference vanishes, and the phase difference then simplifies to

$$\Phi_{ij}^{(0)} = \frac{\Delta m_{ij}^2 (x - x_0)}{2E_\nu}.\quad (40)$$

So, a non-universal coupling to torsion is necessary to have observable effects, as it is the coupling difference $\Delta \kappa^{(ij)}$ that drives the deviation from standard neutrino oscillations.

To apply this general result to a physical scenario, such as neutrino propagation from the surface of the Sun, a specific model for the component $T_1(x)$ is required. By adopting the obtained torsion profile (Eq.(18)), the phase difference in vacuum can be expressed as

$$\begin{aligned}\Phi_{ij}(R) &= \frac{\Delta m_{ij}^2 R_\odot (R - 1)}{2E_\nu} \\ &+ \Delta \kappa^{(ij)} \left[\frac{(R - 1) (3GM_\odot R R_\odot + 64\alpha(R + 1))}{R^2 R_\odot^2} + 4 \ln(R) \right].\end{aligned}\quad (41)$$

The second term includes the geometric and gravitational contributions of the torsion.

From a physical standpoint, these results suggest that spacetime torsion acts as an effective medium through which neutrinos propagate, altering their kinematics without invoking new particle interactions (non-standard interactions). The torsion-induced terms can be viewed as a gravitationally generated background field that distinguishes between neutrino mass eigenstates through the coupling constants $\kappa^{(i)}$. This opens the possibility of flavor-dependent gravitational effects and provides a mechanism through which modified gravity theories may leave observable imprints in neutrino oscillation experiments.

3.2 Modified Matter Effects

The MSW effect [16, 17] emerges from the interplay between two key phenomena: the vacuum oscillations of neutrinos and their coherent forward scattering with electrons in matter with varying density, leading to resonant enhancement of flavor conversion. Electron-neutrinos experience an additional potential $V(x) = \sqrt{2}G_F N_e$, where G_F is Fermi's constant and N_e is electron number density, which creates an effective mass difference. Including the $\nu_e - e^-$ weak interactions, the torsion-induced Schrödinger-like equation (34) can be re-written as

$$i \frac{dh_i(x)}{dx} = \frac{\hat{m}_i^2}{2\hat{E}_\nu} h_i(x) + V(x) U_{ei} U_{ej}^* h_j(x), \quad (42)$$

for the case inside matter. Without loss of generality, we have

$$i \frac{d}{dr} \begin{pmatrix} h_1 \\ h_2 \\ h_3 \end{pmatrix} = \frac{1}{2\hat{E}_\nu} \begin{pmatrix} 2\hat{E}_\nu V(r) c_{12}^2 c_{13}^2 & 2\hat{E}_\nu V(r) c_{12} s_{12} c_{13}^2 & 2\hat{E}_\nu V(r) c_{12} c_{13} s_{13} \\ 2\hat{E}_\nu V(r) c_{12} s_{12} c_{13}^2 & 2\hat{E}_\nu V(r) s_{12}^2 c_{13}^2 + \Delta\hat{m}_{21}^2 & 2\hat{E}_\nu V(r) s_{12} c_{13} s_{13} \\ 2\hat{E}_\nu V(r) c_{12} c_{13} s_{13} & 2\hat{E}_\nu V(r) s_{12} c_{13} s_{13} & 2\hat{E}_\nu V(r) s_{13}^2 + \Delta\hat{m}_{31}^2 \end{pmatrix} \begin{pmatrix} h_1 \\ h_2 \\ h_3 \end{pmatrix}, \quad (43)$$

where, neglecting the term proportional to $\mathcal{O}(\kappa^{(i)^2} T_1^2)$ in (36), we have defined $\Delta\hat{m}_{ij}^2(r) \simeq \Delta m_{ij}^2 - 2E_\nu \Delta\kappa^{(ij)} T_1(r)$ as the torsion-induced mass-squared difference. As previously stated, we restricted our analysis to directions that lie exactly on the x -axis in equatorial plane, where the radial distance is $x = r$. For such a case, we set $(\theta_{\text{polar}}, \phi_{\text{azimuthal}}) = (\pi/2, 0)$.

The effective mass and mixing parameters for neutrinos inside matter with background torsion are derived from the eigenvalues and eigenvectors, obtained by diagonalizing the effective Hamiltonian. A common approximation for many experiments is the two-flavor scenario. For solar neutrinos, the condition $|\Delta\hat{m}_{31}^2| \gg 2\hat{E}_\nu V(r)$ holds, allowing flavor transitions to be described by an effective two-neutrino model, with the third eigenstate decoupling from the other two [75, 76]. Therefore, the effective Hamiltonian governing the propagation of neutrinos through matter is reduced to

$$\mathcal{H}_m = \frac{1}{4\hat{E}_\nu} \left[\Delta\hat{m}^2 \begin{pmatrix} -\cos 2\theta & \sin 2\theta \\ \sin 2\theta & \cos 2\theta \end{pmatrix} + 2\hat{E}_\nu V(r) \begin{pmatrix} 1 & 0 \\ 0 & -1 \end{pmatrix} \right], \quad (44)$$

where $\Delta\hat{m}^2 \equiv \Delta\hat{m}_{21}^2$ for 2ν -case. Then, the resulting neutrino oscillation parameters, after accounting for the torsion-induced couplings, are

$$\Delta m_m^2 = \Delta\hat{m}^2 \sqrt{\sin^2 2\theta + \left[\cos 2\theta - \frac{2\hat{E}_\nu V(r)}{\Delta\hat{m}^2} \right]^2}, \quad (45)$$

and

$$\sin 2\theta_m = \frac{\sin 2\theta}{\sqrt{\sin^2 2\theta + \left[\cos 2\theta - \frac{2\hat{E}_\nu V(r)}{\Delta\hat{m}^2} \right]^2}}. \quad (46)$$

These key oscillation parameters are naturally influenced by the Sun’s electron number density. Moving forward, it is simpler to treat neutrinos as if they were in a vacuum, but with re-defined mass and mixing parameters Δm_m^2 and θ_m . It is evident that, even in vacuum, where the electron density N_e approaches zero, the presence of torsion modifies the neutrino mass-squared splitting, i.e., $\Delta m_m^2 \rightarrow \Delta \hat{m}^2 \neq \Delta m^2$. For the allowed ranges $|\alpha| \lesssim 5m^2$ the torsion-induced correction to Δ_{31}^2 is negligible compared to its vacuum value ($\sim 2.5 \times 10^{-3} eV^2$), so the two-flavor approximation remains valid for solar neutrinos.

4 Numerical Results

In the context of $f(T)$ gravity, spacetime torsion couples directly to neutrino spinor fields, leading to an additional term in the neutrino equation of motion, see Section 3. This coupling can be reinterpreted as an effective shift in both the neutrino energy and mass-squared eigenvalues. The resulting modifications alter the oscillation phases in a manner analogous to matter-induced effects, but with a purely geometric origin, see Subsection 3.1. At leading order, the torsion-induced correction introduces an energy-dependent contribution to the neutrino mass spectrum, which may generate observable deviations from standard oscillation predictions. Unlike the MSW effect or non-standard interactions in matter, these corrections persist in vacuum and reflect properties of spacetime torsion through the higher-order terms in $f(T) = T + \alpha T^k$. Consequently, neutrino oscillations provide a sensitive probe of teleparallel gravity effects, potentially allowing constraints on torsion couplings from current and future neutrino experiments.

For the numerical calculations in this study, we use the neutrino mass and mixing parameters obtained from the NuFit-6.0 global analysis [77], which are listed in Table 1. These values incorporate the latest experimental constraints from oscillation data, including reactor, accelerator, and solar neutrino measurements, ensuring consistency with current phenomenological benchmarks.

Although numerous experiments are designed to study matter-affected neutrino oscillations to probe beyond-Standard Model physics, solar neutrinos currently provide an experimentally confirmed platform for observing significant matter effects.

Table 1: The global fit of three-flavor oscillation parameters at the best-fit and 1σ confidence level, performed by NuFit-6.0 [77]. The SK+SNO and KamLAND data are taken from [78, 79].

	$\sin^2(\theta_{12})$	$\Delta m_{21}^2 [10^{-5} eV^2]$
SK+SNO [78, 79]	$0.306^{+0.014}_{-0.014}$	$6.11^{+1.21}_{-0.68}$
KamLAND [78, 79]	$0.316^{+0.034}_{-0.026}$	$7.54^{+0.19}_{-0.18}$
Combined (NuFit-6.0) [77]	$0.308^{+0.012}_{-0.011}$	$7.49^{+0.19}_{-0.19}$

We begin by investigating the influence of various neutrino-torsion coupling strengths on oscillation phenomena in vacuum. Figure 1 demonstrates the qualitative consequences of varying the coupling difference parameter, $\Delta\kappa^{(ij)}$. The plot clearly indicates that larger $\Delta\kappa^{(ij)}$ values result in a suppression of the oscillation amplitude, an effect that becomes more pronounced at higher neutrino energies.

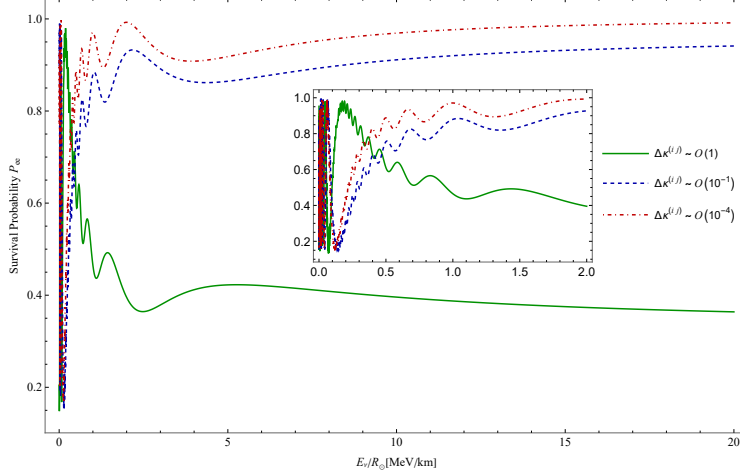


Figure 1: This figure displays the ν_e survival probability in vacuum as a function of E_ν/R_\odot for different $\Delta\kappa^{(ij)}$ values, with α fixed at $\mathcal{O}(1 m^2)$.

Furthermore, the torsion-neutrino coupling introduces an energy-dependent shift in $\Delta\hat{m}^2$ (see Eq.(36)), with a deviation occurring at the solar surface for ${}^8\text{B}$ neutrinos (with $E_\nu \simeq 10$ MeV). It is important to note that this analysis does not include matter potential effects on $\Delta\hat{m}^2$. This modification tends to the vacuum value on the Earth, i.e., $7.49 \times 10^{-5} \text{eV}^2$, consistent with large mixing angle (LMA) parameters. The right panel of Figure 2 (for $|\Delta\kappa^{(ij)}| \sim \mathcal{O}(10^{-2})$) reveals weaker but probably non-negligible corrections to the mass-squared splitting, suggesting detectability in high-precision future experiments. Note that solid and dashed curves correspond to positive and negative values of $\Delta\kappa^{(ij)}$, respectively. As the plot indicates, a positive coupling difference (solid curves) results in a descending mass-squared splitting, while a negative coupling difference (dashed curves) produces an ascending trend.

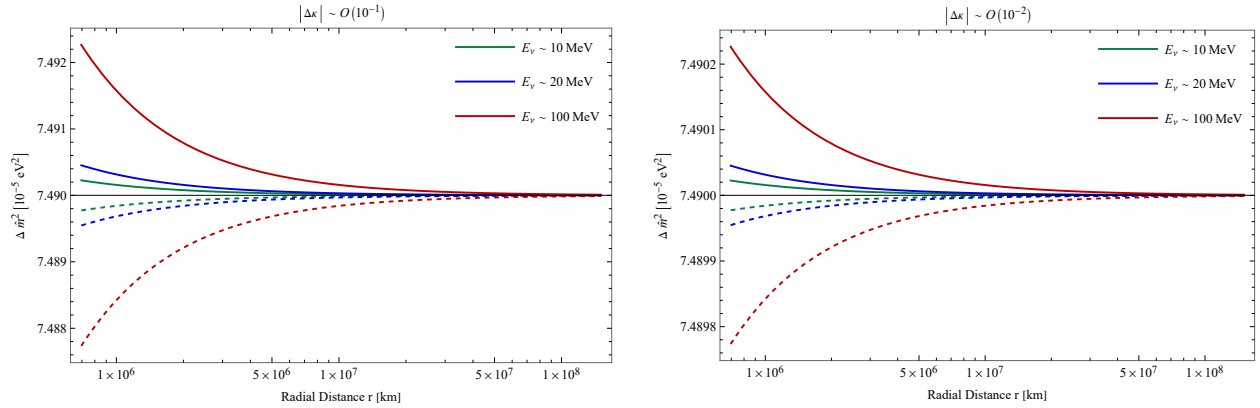


Figure 2: Radial and energy dependence of the effective solar mass-squared splitting. The mass-squared splitting tends toward the solar surface for higher-energy neutrinos, converging to a constant value, corresponding to the LMA solution (cf. Table 1). This behavior reflects torsion-induced modifications to neutrino oscillations in vacuum. We have set the model parameter $\alpha \sim \mathcal{O}(1 m^2)$ and two possible values for the coupling difference $|\Delta\kappa^{(ij)}| \sim \mathcal{O}(10^{-1})$ (left panel) and $|\Delta\kappa^{(ij)}| \sim \mathcal{O}(10^{-2})$ (right panel). Solid curves represent positive $\Delta\kappa^{(ij)}$ values, and dashed curves represent negative ones.

We show the predictions of survival probability $P_{ee}(E_\nu)$ for solar neutrinos, spanning the energy regime from the lowest-energy pp to the higher-energy ${}^8\text{B}$ neutrinos. Once passing through the dense region inside matter, the neutrino state is determined by the comparison between $\cos 2\theta$ and $\frac{2\hat{E}_\nu V(r_0)}{\Delta\hat{m}^2}$, evaluated at the neutrino's production point r_0 . The predicted survival probability can fall into three regimes:

- $\cos 2\theta \gg \frac{2\hat{E}_\nu V(r_0)}{\Delta\hat{m}^2}$: For low-energy pp neutrinos, where matter effects are negligible, neutrino propaga-

tion follows the vacuum oscillation pattern, yielding an averaged electron survival probability of $P_{ee} \simeq 0.55$. In the present model, this vacuum-dominated regime may occur for $|\alpha| \gtrsim 100 m^2$ or $|\Delta\kappa| \gtrsim 0.1$, as shown in Figs. 3 and 4, rendering the oscillation behavior of all solar neutrinos energy-independent.

However, comparison with Borexino data imposes constraints on the torsional parameter α . While enhanced matter effects significantly suppress the survival probability for higher-energy ${}^8\text{B}$ neutrinos—effectively restoring vacuum oscillations at large $f(T)$ parameters ($|\alpha| \gtrsim 100 m^2$)—the model’s disagreement with observations restricts the model parameter to the range $-2 \lesssim \alpha[m^2] \lesssim 3$.

■ $\cos 2\theta \gtrsim \frac{2\hat{E}_\nu V(r_0)}{\Delta\hat{m}^2}$: For this case, we encounter the neutrino mixing, modified by matter effects, which can be effectively modeled using adiabatic propagation. Here, the survival probability for solar electron-neutrinos is given by

$$P_{ee}(E_\nu) = \frac{1}{2} [1 + \cos 2\theta \cos 2\theta_m]. \quad (47)$$

It is predicted that the torsion-induced effects might be considerable for this case, i.e., for ${}^8\text{B}$ neutrinos with energy of around ~ 10 MeV, as they have intersections with the standard matter effects (gray bands with 1σ C.L. in Figs.3 and 4). In a similar manner, the probability that an electron-neutrino will change its flavor to muon-neutrino during propagation is described by

$$P_{e\mu}(E_\nu) = \frac{1}{2} [1 - \cos 2\theta \cos 2\theta_m]. \quad (48)$$

The observed solar neutrino deficit—a lower-than-expected detection of electron -neutrinos from the Sun—was solved by the discovery of neutrino oscillations. This process allows neutrinos to change flavors during their journey to Earth, diminishing the number that remain as electron-neutrinos.

■ $\cos 2\theta < \frac{2\hat{E}_\nu V(r_0)}{\Delta\hat{m}^2}$: For higher-energy neutrinos, they can cross the resonance region. The ν_e survival probability is approximately $P_{ee} \simeq 0.33$ for this situation.

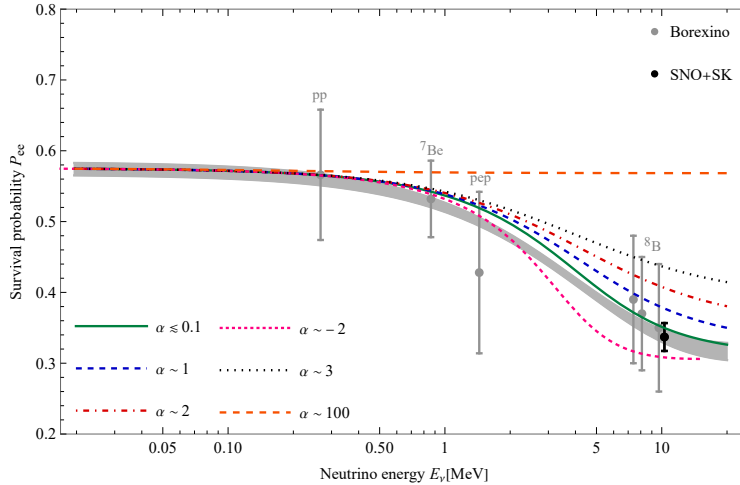


Figure 3: Transition between matter and vacuum-dominated neutrino oscillation regimes. This figure is plotted for various values of the model parameter α (in units m^2). We have assumed that $\Delta\kappa \simeq 0.001$. The observational data are taken from Borexino [69] (gray points) and SNO+SK [80] (a single black point).

To quantify the goodness-of-fit in probability space, the chi-square (χ^2) analysis is calculated using the formula

$$\chi^2 = \sum_i \frac{(P_i^{\text{obs}} - P_i^{\text{th}})^2}{\sigma_i^2}. \quad (49)$$

Here, P_i^{obs} and σ_i are the observed central values and uncertainties from the data (in Figs. 3 and 4), and P_i^{th} is the theoretically predicted value, obtained by the present model. We determined the optimal (best-fit)

values of the model parameters by finding the values of α and $\Delta\kappa$ that minimize the χ^2 value against the experimental data. The corresponding 1σ and 2σ confidence intervals are determined by the parameter regions where $\Delta\chi^2 = \chi^2 - \chi_{\text{bf}}^2$ does not exceed 1.0 and 4.0, respectively. In this framework, all experimental uncertainties are treated as independent statistical errors; no correlated systematic effects across experiments or data releases are incorporated. The analysis does not impose external theoretical priors on the model parameters α and $\Delta\kappa$; constraints arise exclusively from the solar neutrino data likelihood.

Table 2 summarizes constraints on the $f(T)$ gravity parameter α inferred from measurements of the solar ^8B neutrino flux by several generations of solar neutrino experiments. The table reports, for each experiment or combination of experiments, the experimentally measured electron-neutrino flux and the corresponding best-fit value of α , together with its 1σ and 2σ confidence intervals within the framework of the present model.

The Kamiokande [81] result yields a best-fit value $\alpha_{\text{bf}} = 0.22$ with relatively broad 1σ and especially 2σ confidence intervals, implying its limited statistical precision compared to later experiments. Therefore, Kamiokande provides only weak constraints on α and is fully consistent with $\alpha = 0$ limit.

A general observation is that experiments with higher statistical precision, notably the SK phases I-IV [4, 82–84], yield comparatively tight constraints on α . Individually, the SK phases favor positive best-fit values of α of order $\mathcal{O}(1 m^2)$, with best fits ranging from $\alpha_{\text{bf}} \simeq 0.55$ to 0.89. Importantly, all individual SK measurements are statistically consistent with $\alpha = 0$ at the 1σ level, as their confidence intervals include zero. The combined SK analysis (global-SK) significantly sharpens these constraints, reducing the allowed parameter space to $[-0.03, 1.19]$ at 1σ and $[-0.62, 1.95]$ at 2σ . This highlights the strong constraining power of homogeneous, high-statistics datasets and suggests only mild deviations from the standard teleparallel gravity limit.

In contrast, SNO [85–87] results display a marked dependence on the detection channel. Charged-current (CC) measurements across all SNO phases consistently favor large negative best-fit values, $\alpha_{\text{bf}} \simeq -5.52$, which appear to saturate the lower boundary of the parameter space explored. Their 1σ intervals lie entirely in the negative- α region, indicating tension with both $\alpha = 0$ and the SK-preferred values. However, the corresponding 2σ intervals extend into positive α values, implying that this tension is not decisive at higher confidence levels. By contrast, SNO measurements based on νe scattering yield best-fit values of α close to zero or mildly positive and are broadly compatible with SK results within uncertainties. The global-SNO fit (restricted to νe phases) shows a positive best-fit value $\alpha_{\text{bf}} \simeq 4.55$ but is accompanied by very wide confidence intervals, reflecting the comparatively large experimental uncertainties of these channels.

The combined SK+SNO analysis yields a best-fit value $\alpha_{\text{bf}} \simeq 1.38$, with a 1σ interval that is entirely positive. This result indicates that, when the dominant datasets are combined, the data exhibit a mild preference for positive α , although $\alpha \rightarrow 0$ remains allowed at the 2σ level.

The Borexino [69, 88] measurement, characterized by intermediate precision, provides weaker constraints: its best-fit value is negative $\alpha_{\text{bf}} \simeq -1.07$, but both its 1σ and 2σ ranges include zero, rendering it consistent with both standard teleparallel gravity (with $\alpha = 0$) and modest deviations (with $\alpha \neq 0$).

Table 2: Results from solar neutrino experiments regarding ^8B neutrino flux. Best-fit values and 1σ and 2σ confidence intervals for the model parameter α (in m^2) for the present model.

Experiment	ν_e flux [$10^6/\text{cm}^2\text{s}$]	α best-fit	1σ range	2σ range
Kamiokande [81]	2.80 ± 0.19	+0.22	$[-0.56, +2.21]$	$[-1.12, +45.7]$
SK-I [82]	2.38 ± 0.02	+0.74	$[-0.49, +2.24]$	$[-2.28, +4.73]$
SK-II [83]	2.41 ± 0.05	+0.89	$[-0.36, +2.51]$	$[-1.96, +5.33]$
SK-III [84]	2.32 ± 0.04	+0.55	$[-0.73, +2.02]$	$[-3.01, +4.26]$
SK-IV [4]	$+2.31 \pm 0.02$	+0.61	$[-0.69, +2.07]$	$[-3.09, +4.24]$
Global-SK (SK I-IV)		+0.55	$[-0.03, +1.19]$	$[-0.62, +1.95]$
SNO-Phase I (CC) [85]	$1.76^{+0.06}_{-0.05}$	-5.53	$[-5.52, -1.19]$	$[-5.52, +1.50]$
SNO-Phase I (νe) [85]	$2.39^{+0.24}_{-0.23}$	+0.67	$[-0.94, +2.77]$	$[-2.86, +7.64]$
SNO-Phase II (CC) [86]	1.68 ± 0.06	-5.52	$[-5.52, -1.93]$	$[-5.52, +0.66]$
SNO-Phase II (νe) [86]	2.35 ± 0.22	+0.80	$[-1.01, +3.01]$	$[-3.11, +7.59]$
SNO-Phase III (CC) [87]	$1.67^{+0.05}_{-0.04}$	-5.52	$[-5.52, -2.10]$	$[-5.52, +0.43]$
SNO-Phase III (νe) [87]	$1.77^{+0.24}_{-0.21}$	-5.52	$[-5.52, +0.18]$	$[-5.52, +4.10]$
Global-SNO (only νe phases)		+4.55	$[-2.17, +10.3]$	$[-11.6, +16.7]$
SK+SNO		+1.38	$[-0.55, +2.24]$	$[-0.31, +3.19]$
Borexino [69, 88]	$2.57^{+0.17}_{-0.18}$	-1.07	$[-5.33, +1.86]$	$[-9.80, +4.47]$
Global-fit		+2.47	$[-1.09, +3.81]$	$[-0.41, +5.14]$

Finally, the global-fit including all experiments yields a best-fit value $\alpha_{\text{bf}} \simeq 2.47$, with a 1σ interval

[1.09, 3.81] that excludes $\alpha = 0$. This suggests an overall preference for a positive, nonvanishing $f(T)$ gravity parameter when all available solar neutrino data are considered simultaneously. Nevertheless, the 2σ interval $[-0.41, 5.14]$ still includes $\alpha = 0$, indicating that the evidence for deviations from the standard scenario remains suggestive rather than conclusive.

In summary, Table 2 demonstrates that higher-precision solar neutrino measurements, particularly from Super-Kamiokande, place stringent bounds on α , while channel-dependent effects in SNO introduce some tension and broaden the global parameter space. The combined analyses mildly favor positive values of α , but the standard teleparallel gravity limit remains statistically viable at the 2σ level.

Also, we may compare the constraints on the model parameter α with findings from some gravitational experiments. Stringent constraints on α are derived from observed secular variations in planetary orbits. While a previous study [54] calculated a bound of $|\alpha| \lesssim 1.8 \times 10^4 m^2$ from the orbits of the inner solar system planets, current and more precise analyses of these orbital perturbations have significantly tightened this constraint to $|\alpha| \leq 1.2 \times 10^2 m^2$ [64]. A further refinement of this limit arises from independent orbital dynamics studies, with [52] reporting a significantly tighter constraint of $|\alpha| \leq 2.3 \times 10 m^2$. The limits of α derived from our analysis are consistent with these reported constraints, as we have mostly obtained $|\alpha| \lesssim 5 m^2$, see Table 2.

We also investigate the impact of modified matter effects on neutrino flavor transitions by computing the electron-neutrino survival probability across a range of coupling differences $\Delta\kappa$, see Figure 4. This analysis explores how the coupling strength parameter $\Delta\kappa$ modifies neutrino flavor transitions with four regimes:

- For $0 < \Delta\kappa < 10^{-4}$, the curves imply standard MSW behavior with minimal deviations.
- The transitional regime ($10^{-4} \lesssim \Delta\kappa \lesssim 2 \times 10^{-3}$) shows nonlinear effects like shifted resonances, offering optimal sensitivity to the present model.
- The system exhibits oscillations in vacuum as a result of strong coupling differences, typically defined by values of $\Delta\kappa \gtrsim \mathcal{O}(0.1)$.
- Finally, negative coupling differences ($\Delta\kappa < 0$) lead to a suppression of P_{ee} (pink-dashed curve), again indicating the dominance of the new neutrino–torsion coupling.

These effects stem from $\Delta\kappa$'s role in scaling the matter potential, with positive/negative values enhancing or suppression conventional oscillations. Current solar neutrino data constrain $|\Delta\kappa| \lesssim 2 \times 10^{-3}$, while future experiments like JUNO [89] may impose tighter constraints.

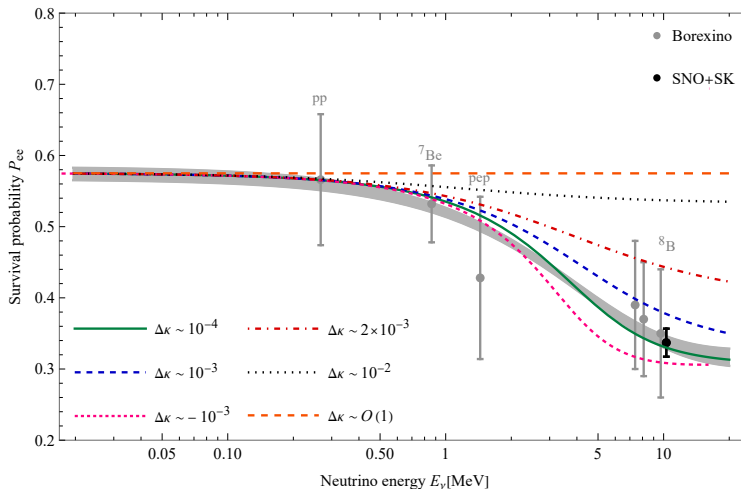


Figure 4: This figure displays P_{ee} versus neutrino energy E_ν for various selected $\Delta\kappa$ values and for $\alpha \sim \mathcal{O}(1 m^2)$.

Table 3 presents constraints on the neutrino-torsion coupling difference $\Delta\kappa$ [10^{-4}], as inferred from flux measurements by a variety of solar neutrino experiments. For each dataset, as in the previous case, the table reports the best-fit value of $\Delta\kappa$ together with its corresponding 1σ and 2σ confidence intervals within the adopted theoretical framework.

The earliest Kamiokande measurement yields a comparatively large best-fit value, $\Delta\kappa_{\text{bf}} \simeq 4.9 \times 10^{-3}$, and provides only a lower bound on the parameter. The absence of an upper constraint and the relatively high

best-fit value reflect the limited statistical precision of this experiment, implying that Kamiokande alone has weak discriminatory power and indicates that sizable values of $\Delta\kappa$ cannot be excluded.

The SK phases I-IV exhibit remarkable internal consistency. Individually, all SK phases favor positive best-fit values of $\Delta\kappa_{\text{bf}}$ around $(1.5 - 1.7) \times 10^{-3}$, with overlapping confidence intervals. While the 2σ ranges of the individual phases extend into negative values, their 1σ intervals remain strictly positive, suggesting a mild but systematic preference for nonzero $\Delta\kappa$. This preference is significantly reinforced in the combined SK analysis, which yields $\Delta\kappa = (1.69^{+0.58}_{-0.53}) \times 10^{-3}$ at 1σ . Notably, the global-SK 2σ interval remains entirely positive, effectively implying $\Delta\kappa \neq 0$ within this dataset.

Results from SNO again display a strong dependence on the detection channel. The CC measurements across all SNO phases converge to a common best-fit value, $\Delta\kappa_{\text{bf}} \simeq 6.2 \times 10^{-4}$, with relatively narrow upper bounds but confidence intervals that include $\Delta\kappa = 0$ at the 1σ or 2σ level. In contrast, the SNO νe scattering prefer larger and positive best-fit values comparable to those from SK, albeit with substantially broader uncertainties. When all SNO data are combined, the resulting global-SNO constraint yields a small positive best-fit value, $\Delta\kappa_{\text{bf}} \simeq 2.5 \times 10^{-4}$, which remains compatible with zero within 1σ , indicating that SNO alone does not provide decisive evidence for a nonvanishing coupling difference.

The combined SK+SNO analysis leads to a best-fit value $\Delta\kappa_{\text{bf}} \simeq 9.8 \times 10^{-4}$, with relatively tight confidence intervals that are strictly positive even at the 2σ level. This result reflects the dominant statistical weight of the high-precision SK data while incorporating the complementary information from SNO, and it strengthens the indication of a positive neutrino-torsion coupling difference.

The Borexino measurement, characterized by larger experimental uncertainties, yields a small best-fit value and extremely wide confidence intervals that span both positive and negative values over a broad range. Consequently, Borexino places only weak constraints on $\Delta\kappa$ and remains fully consistent with both the null hypothesis and the values favored by SK and SK+SNO.

Finally, the global-fit including all experiments yields a positive best-fit value $\Delta\kappa_{\text{bf}} \simeq 4.1 \times 10^{-4}$, with a 1σ interval that excludes zero $\Delta\kappa$. Even at the 2σ level, the allowed range remains strictly positive. This global result therefore provides overall evidence, albeit moderate, for a nonzero neutrino-torsion coupling difference, primarily driven by the high-precision SK data and their consistency across multiple phases.

Table 3: Constraints on neutrino-torsion coupling difference $\Delta\kappa$ (in units of 10^{-4}), showing best-fit values with 1σ and 2σ confidence intervals.

Experiment	ν_e flux [$10^6/\text{cm}^2\text{s}$]	$\Delta\kappa$ best-fit [10^{-4}]	1σ range [10^{-4}]	2σ range [10^{-4}]
Kamiokande [81]	2.80 ± 0.19	48.95	> 24.08	> 6.300
SK-I [82]	2.38 ± 0.02	16.33	[6.620, 28.28]	[-7.540, 47.92]
SK-II [83]	2.41 ± 0.05	16.49	[7.160, 28.48]	[-4.680, 49.46]
SK-III [84]	2.32 ± 0.04	15.46	[4.880, 27.52]	[-13.86, 45.90]
SK-IV [4]	2.31 ± 0.02	14.77	[4.900, 25.92]	[-13.42, 42.44]
Global-SK (SK I-IV)		16.94	[11.64, 22.74]	[6.380, 29.52]
SNO-Phase I (CC) [85]	$1.76^{+0.06}_{-0.05}$	6.217	[-0.220, 6.200]	[-4.200, 6.200]
SNO-Phase I (νe) [85]	$2.39^{+0.24}_{-0.23}$	16.97	[3.280, 34.84]	[-13.06, 76.22]
SNO-Phase II (CC) [86]	1.68 ± 0.06	6.217	[0.900, 6.200]	[-2.940, 6.200]
SNO-Phase II (νe) [86]	2.35 ± 0.22	14.67	[2.140, 29.98]	[-12.28, 61.64]
SNO-Phase III (CC) [87]	$1.67^{+0.05}_{-0.04}$	6.217	[1.140, 6.200]	[-2.600, 6.200]
SNO-Phase III (νe) [87]	$1.77^{+0.24}_{-0.21}$	6.217	[-2.240, 6.200]	[-8.040, 6.200]
Global-SNO		2.534	[-0.360, 5.020]	[-4.420, 7.780]
SK+SNO		9.781	[6.780, 12.90]	[3.700, 16.34]
Borexino [69, 88]	$2.57^{+0.17}_{-0.18}$	2.996	[-46.64, 37.24]	[-98.50, 67.50]
Global-fit		4.082	[2.600, 5.500]	[0.9800, 6.940]

Figure 5(a) illustrates the dependence of the electron-neutrino survival probability P_{ee} on the parameter α for 10 MeV ${}^8\text{B}$ neutrinos, comparing with experimental results from several detectors (SNO, SK, Borexino, Kamiokande) and global-fits (shown by the asterisks in the plot). As α increases, matter-induced effects encoded in the $f(T)$ framework become progressively suppressed, leading to a smooth rise in P_{ee} . In the regime $\alpha \gg 1 m^2$, the survival probability saturates at $P_{ee} \simeq 0.55$, indicating the recovery of the vacuum oscillation limit. The agreement with global solar neutrino data further supports the physical viability of the chosen parameter range.

Figure 5(b) presents the dependence of the electron-neutrino survival probability P_{ee} on the coupling difference $\Delta\kappa[10^{-3}]$. For very small coupling differences $\Delta\kappa \ll 1$, the survival probability attains its minimum, indicating a regime dominated by standard matter effects. As $\Delta\kappa$ increases, deviations induced by the modified coupling become significant, leading to a systematic enhancement of P_{ee} . This trend reflects

the growing influence of profile-dependent corrections in the neutrino propagation dynamics.

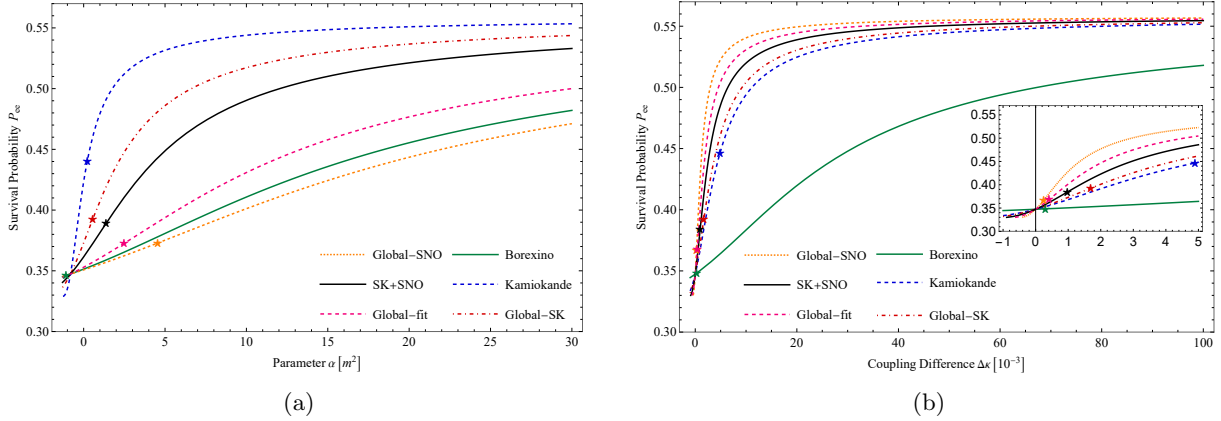


Figure 5: (a) Matter-to-vacuum transition in neutrino oscillations under $f(T)$ gravity. The plot displays the evolution of the survival probability P_{ee} across varying strengths of the model parameter $\alpha[m^2]$, for each observational dataset. (b) P_{ee} as a function of the coupling difference $\Delta\kappa[10^{-3}]$.

Figure 6 illustrates the survival probability P_{ee} , comparing different values of the parameters α (left panel) and $\Delta\kappa$ (right panel). The model assumes that the torsion effects caused by an average constant Earth density and is computed using the KamLAND best-fit mass and mixing parameters (see Table 1), resulting in deviations in the standard MSW effect pattern. Based on the experimental solar data from Borexino [69] (data points in the plots), the most plausible constraints on these parameters are estimated to be $|\alpha| \lesssim 5.5 m^2$ and $|\Delta\kappa| \lesssim 0.006$. These bounds are consistent with the findings in Tables 2 and 3; any deviation beyond them conflicts with experimental evidence.

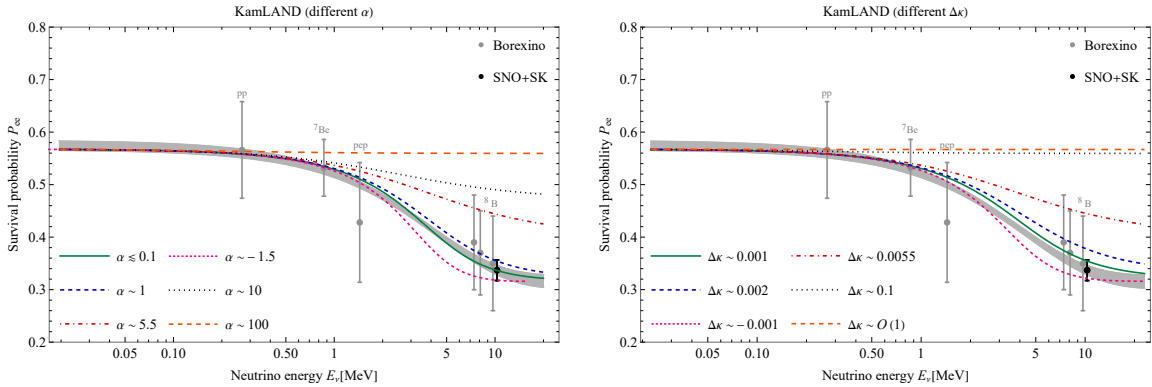


Figure 6: Electron-neutrino survival probability as a function of energy for (left) varying $\alpha[m^2]$ and (right) varying $\Delta\kappa$, for the KamLAND's best-fit oscillation parameters from Table 1.

5 Conclusion

This work has established a theoretical framework within $f(T)$ gravity (see Section 2) to quantify the impact of spacetime torsion on neutrino flavor change. We have derived general, analytical expressions that describe how torsion induces a measurable phase shift and neutrino wavefunction, see Section 3. Crucially, these modifications affect both the vacuum oscillation paradigm (Subsection 3.1) and the standard MSW resonance mechanism in matter (Subsection 3.2). Our analysis, applied to the polynomial density profile, demonstrates that the gravitational torsion might have a non-negligible effect in various environments and presents a new mechanism for flavor conversion.

The formalism provides a direct link between the geometric formulation of gravity and quantum particle phenomenology. This paper demonstrates a method for investigating theories beyond teleparallel equivalent of general relativity. It establishes calculations of neutrino behavior in astrophysical environments as a possibility for testing higher-order terms of torsion in $f(T)$ gravity. The analysis places stringent limits on the key parameter α of this model, finding mostly $|\alpha| \lesssim 5 m^2$ (2σ allowed ranges from the numerical results are given in Table 2). Our constraints on α from solar neutrinos are stronger than those from planetary orbits, reflecting the high sensitivity of quantum interferometric phenomena to small geometric perturbations over astronomical distances. This result is consistent with constraints from other studies [52–54], which found $|\alpha| \lesssim 23 m^2$ for the most stringent one. Future work will involve applying these constraints to specific astrophysical objects and refining the predictions for next-generation neutrino observatories.

Acknowledgement

This work is based upon research funded by Iran National Science Foundation (INSF) under project No. 4036948.

References

- [1] B. Pontecorvo, Sov. Phys. JETP **6**, 429 (1957).
- [2] A. B. McDonald, Rev. Mod. Phys. **88**, 030502 (2016).
- [3] A. Bellerive et al. [SNO Collaboration], Nucl. Phys. B **908**, 30 (2016) [arXiv:1602.02469 [nucl-ex]].
- [4] Y. Fukuda *et al.* [Super-Kamiokande], Nucl. Instrum. Meth. A **501**, 418-462 (2003).
- [5] Q. R. Ahmad *et al.* [SNO], Phys. Rev. Lett. **89**, 011301 (2002) [arXiv:nucl-ex/0204008 [nucl-ex]].
- [6] B. Aharmim *et al.* [SNO], Phys. Rev. Lett. **101**, 111301 (2008) [arXiv:0806.0989 [nucl-ex]].
- [7] K. Abe *et al.* [Super-Kamiokande], Phys. Rev. D **83**, 052010 (2011) [arXiv:1010.0118 [hep-ex]].
- [8] B. Aharmim *et al.* [SNO], Phys. Rev. C **88**, 025501 (2013) [arXiv:1109.0763 [nucl-ex]].
- [9] K. Abe *et al.* [Super-Kamiokande], Phys. Rev. D **94**, 052010 (2016) [arXiv:1606.07538 [hep-ex]].
- [10] M. G. Aartsen *et al.* [IceCube], Phys. Rev. D **91**, 072004 (2015) [arXiv:1410.7227 [hep-ex]].
- [11] K. Abe *et al.* [Super-Kamiokande], Phys. Rev. D **97**, 072001 (2018) [arXiv:1710.09126 [hep-ex]].
- [12] M. Jiang *et al.* [Super-Kamiokande], PTEP **2019**, 053F01 (2019) [arXiv:1901.03230 [hep-ex]].
- [13] D. Adey *et al.* [Daya Bay], Phys. Rev. Lett. **121**, 241805 (2018) [arXiv:1809.02261 [hep-ex]].
- [14] G. Bak *et al.* [RENO], Phys. Rev. Lett. **121**, 201801 (2018) [arXiv:1806.00248 [hep-ex]].
- [15] P. Adamson *et al.* [MINOS], Phys. Rev. Lett. **112**, 191801 (2014) [arXiv:1403.0867 [hep-ex]].
- [16] S. P. Mikheyev, A. Yu. Smirnov, Sov. J. Nucl. Phys. **42**, 913 (1985).
- [17] L. Wolfenstein, Phys. Rev. D **20**, 2634 (1979).
- [18] C. Y. Cardall and G. M. Fuller, Phys. Rev. D **55**, 7960-7966 (1997) [arXiv:hep-ph/9610494 [hep-ph]].
- [19] N. Fornengo, C. Giunti, C. W. Kim and J. Song, Phys. Rev. D **56**, 1895 (1997) [arXiv:hep-ph/9611231 [hep-ph]].
- [20] L. Visinelli, Gen. Rel. Grav. **47**, 62 (2015) [arXiv:1410.1523 [gr-qc]].
- [21] S. Chakraborty, JCAP **10**, 019 (2015) [arXiv:1506.02647 [gr-qc]].

- [22] H. Mohseni Sadjadi and A. P. Khosravi, JCAP **04**, 008 (2018) [arXiv:1711.06607 [hep-ph]].
- [23] M. Blasone, G. Lambiase, G. G. Luciano and L. Petruzziello, EPL **124**, 51001 (2018) [arXiv:1812.09697 [hep-ph]].
- [24] L. Buoninfante, G. G. Luciano, L. Petruzziello and L. Smaldone, Phys. Rev. D **101**, 024016 (2020) [arXiv:1906.03131 [gr-qc]].
- [25] M. G. Betti *et al.* [PTOLEMY], JCAP **07**, 047 (2019) [arXiv:1902.05508 [astro-ph.CO]].
- [26] R. Fardon, A. E. Nelson and N. Weiner, JCAP **10**, 005 (2004) [arXiv:astro-ph/0309800 [astro-ph]].
- [27] D. B. Kaplan, A. E. Nelson and N. Weiner, Phys. Rev. Lett. **93**, 091801 (2004) [arXiv:hep-ph/0401099 [hep-ph]].
- [28] H. Mohseni Sadjadi and H. Y. Ahmadabadi, Phys. Rev. D **103**, 065012 (2021) [arXiv:2012.03633 [hep-ph]].
- [29] H. Y. Ahmadabadi and H. Mohseni Sadjadi, Phys. Dark Univ. **37**, 101067 (2022) [arXiv:2111.03054 [hep-ph]].
- [30] H. Yazdani Ahmadabadi and H. Mohseni Sadjadi, Phys. Lett. B **850**, 138493 (2024) [arXiv:2201.02927 [hep-ph]].
- [31] H. Yazdani Ahmadabadi and H. Mohseni Sadjadi, Phys. Lett. B **859**, 139110 (2024) [arXiv:2209.13367 [hep-ph]].
- [32] H. Mohseni Sadjadi and H. Yazdani Ahmadabadi, Phys. Lett. B **870**, 139942 (2025) [arXiv:2510.00704 [hep-ph]].
- [33] V. C. De Andrade, L. C. T. Guillen and J. G. Pereira, “Teleparallel gravity: An Overview,” [arXiv:gr-qc/0011087 [gr-qc]].
- [34] R. Aldrovandi and J. G. Pereira, *Teleparallel Gravity: An Introduction*, Springer Dordrecht, (2012).
- [35] H. Mohseni Sadjadi, Phys. Rev. D **87**, 064028 (2013) [arXiv:1302.1180 [gr-qc]].
- [36] H. Mohseni Sadjadi, Phys. Rev. D **92**, no.12, 123538 (2015) [arXiv:1510.02085 [gr-qc]].
- [37] H. Mohseni Sadjadi, JCAP **01**, 031 (2017) [arXiv:1609.04292 [gr-qc]].
- [38] S. Bahamonde *et. al.*, Rep. Prog. Phys. **86** 026901 (2023), [arXiv:2106.13793 [gr-qc]].
- [39] S. Nojiri, S.D. Odintsov and V. K.Oikonomou, Phys. Rept. **692** (2017), 1, [arXiv:1705.11098 [gr-qc]].
- [40] A. G. Riess *et al.* [Supernova Search Team], Astron. J. **116**, 1009-1038 (1998) [arXiv:astro-ph/9805201 [astro-ph]].
- [41] S. Perlmutter *et al.* [Supernova Cosmology Project], Astrophys. J. **517**, 565-586 (1999) [arXiv:astro-ph/9812133 [astro-ph]].
- [42] D. J. Eisenstein *et al.* [SDSS], Astrophys. J. **633**, 560-574 (2005) [arXiv:astro-ph/0501171 [astro-ph]].
- [43] Y. Wang, Phys. Rev. D **78**, 123532 (2008) [arXiv:0809.0657 [astro-ph]].
- [44] R. Weitzenböck, *Invarianten Theorie*, (Nordhoff, Groningen, 1923).
- [45] E. V. Linder, Phys. Rev. D **81**, 127301 (2010) [erratum: Phys. Rev. D **82**, 109902 (2010)] [arXiv:1005.3039 [astro-ph.CO]].
- [46] R. Myrzakulov, Eur. Phys. J. C **71**, 1752 (2011) [arXiv:1006.1120 [gr-qc]].
- [47] R. Ferraro and F. Fiorini, Phys. Rev. D **84**, 083518 (2011) [arXiv:1109.4209 [gr-qc]].

- [48] T. Wang, Phys. Rev. D **84**, 024042 (2011) [arXiv:1102.4410 [gr-qc]].
- [49] C. G. Boehmer, A. Mussa and N. Tamanini, Class. Quant. Grav. **28**, 245020 (2011) [arXiv:1107.4455 [gr-qc]].
- [50] G. G. L. Nashed, Phys. Rev. D **88**, 104034 (2013) [arXiv:1311.3131 [gr-qc]].
- [51] A. Paliathanasis, S. Basilakos, E. N. Saridakis, S. Capozziello, K. Atazadeh, F. Darabi and M. Tsampanlis, Phys. Rev. D **89**, 104042 (2014)[arXiv:1402.5935 [gr-qc]].
- [52] M. L. Ruggiero and N. Radicella, Phys. Rev. D **91**, 104014 (2015) [arXiv:1501.02198 [gr-qc]].
- [53] Y. Xie and X. M. Deng, Mon. Not. Roy. Astron. Soc. **433**, 3584-3589 (2013) [arXiv:1312.4103 [gr-qc]].
- [54] L. Iorio and E. N. Saridakis, Mon. Not. Roy. Astron. Soc. **427**, 1555 (2012) [arXiv:1203.5781 [gr-qc]].
- [55] J. W. Maluf, Annalen Phys. **525**, 339-357 (2013) [arXiv:1303.3897 [gr-qc]].
- [56] S. Bahamonde and M. Wright, Phys. Rev. D **92**, no.8, 084034 (2015) [erratum: Phys. Rev. D **93**, no.10, 109901 (2016)] [arXiv:1508.06580 [gr-qc]].
- [57] S. Bahamonde, C. G. Böhmer and M. Wright, Phys. Rev. D **92**, no.10, 104042 (2015) [arXiv:1508.05120 [gr-qc]].
- [58] I. L. Shapiro, Phys. Rept. **357**, 113 (2002) [arXiv:hep-th/0103093 [hep-th]].
- [59] S. Capozziello and M. Francaviglia, Gen. Rel. Grav. **40**, 357-420 (2008) [arXiv:0706.1146 [astro-ph]].
- [60] T. P. Sotiriou and V. Faraoni, Rev. Mod. Phys. **82**, 451-497 (2010) [arXiv:0805.1726 [gr-qc]].
- [61] N. Tamanini and C. G. Boehmer, Phys. Rev. D **86**, 044009 (2012) [arXiv:1204.4593 [gr-qc]].
- [62] J. N. Bahcall, A. M. Serenelli and S. Basu, Astrophys. J. Lett. **621**, L85-L88 (2005) [arXiv:astro-ph/0412440 [astro-ph]].
- [63] For example, see website: <https://spacemath.gsfc.nasa.gov>
- [64] A. Fienga, J. Laskar, P. Kuchynka, H. Manche, M. Gastineau and C. Leponcin-Lafitte, IAU Symp. **261**, 159-169 (2010) [arXiv:0906.3962 [gr-qc]].
- [65] N.P. Pitjev, E.V. Pitjeva, Astronomy Letters **39**, 141 (2013) [arXiv:1306.5534 [astro-ph.EP]].
- [66] E.V. Pitjeva, Solar System Research **47**, 386 (2013) [arXiv:1308.6416 [astro-ph.EP]].
- [67] E.V. Pitjeva, N.P. Pitjev , MNRAS **432**, 3431 (2013) [arXiv:1306.3043 [astro-ph.EP]].
- [68] Y. Mao, M. Tegmark, A. H. Guth and S. Cabi, Phys. Rev. D **76**, 104029 (2007) [arXiv:gr-qc/0608121 [gr-qc]].
- [69] M. Agostini et al. [BOREXINO], Nature **562**, no.7728, 505 (2018).
- [70] A. Capolupo, G. De Maria, S. Monda, A. Quaranta and R. Serao, Universe **10**, no.4, 170 (2024) [arXiv:2310.09309 [hep-ph]].
- [71] A. Capolupo, S. Monda, G. Pisacane, A. Quaranta and R. Serao, J. Phys. Conf. Ser. **3017**, no.1, 012049 (2025) [arXiv:2503.05851 [hep-ph]].
- [72] E. Akhmedov and A. Trautner, JHEP **05**, 156 (2024) [arXiv:2402.05172 [hep-ph]].
- [73] D. Piriz, M. Roy and J. Wudka, Phys. Rev. D **54**, 1587-1599 (1996) [arXiv:hep-ph/9604403 [hep-ph]].
- [74] W. N. Cottingham and D. A. Greenwood, “An Introduction to the Standard Model of Particle Physics,” Cambridge university press, ISBN-13 978-0-521-85249-4, 2007.

- [75] S. K. Agarwalla *et al.* [Borexino], JHEP **02**, 038 (2020) [arXiv:1905.03512 [hep-ph]].
- [76] P. Martínez-Miravé, S. M. Sedgwick and M. Tórtola, Phys. Rev. D **105**, no.3, 035004 (2022) [arXiv:2111.03031 [hep-ph]].
- [77] I. Esteban, M. C. Gonzalez-Garcia, M. Maltoni, I. Martinez-Soler, J. P. Pinheiro and T. Schwetz, JHEP **12**, 216 (2024) [arXiv:2410.05380 [hep-ph]].
- [78] Y. Nakajima, Neutrino 2020 (neutrino2020) (2020).
- [79] A. Gando *et al.* [KamLAND], Phys. Rev. D **88**, no.3, 033001 (2013) [arXiv:1303.4667 [hep-ex]].
- [80] P. A. Zyla *et al.* [Particle Data Group], PTEP **2020**, 083C01 (2020).
- [81] Y. Fukuda *et al.* [Kamiokande], Phys. Rev. Lett. **77**, 1683-1686 (1996).
- [82] J. Hosaka *et al.* [Super-Kamiokande], Phys. Rev. D **73**, 112001 (2006) [arXiv:hep-ex/0508053 [hep-ex]].
- [83] J. P. Cravens *et al.* [Super-Kamiokande], Phys. Rev. D **78**, 032002 (2008) [arXiv:0803.4312 [hep-ex]].
- [84] K. Abe *et al.* [Super-Kamiokande], Phys. Rev. D **83**, 052010 (2011) [arXiv:1010.0118 [hep-ex]].
- [85] Q. R. Ahmad *et al.* [SNO], Phys. Rev. Lett. **89**, 011301 (2002) [arXiv:nucl-ex/0204008 [nucl-ex]].
- [86] B. Aharmim *et al.* [SNO], Phys. Rev. C **72**, 055502 (2005) [arXiv:nucl-ex/0502021 [nucl-ex]].
- [87] B. Aharmim *et al.* [SNO], Phys. Rev. Lett. **101**, 111301 (2008) [arXiv:0806.0989 [nucl-ex]].
- [88] M. Agostini *et al.* [Borexino], Phys. Rev. D **101**, no.6, 062001 (2020) [arXiv:1709.00756 [hep-ex]].
- [89] F. An *et al.* [JUNO], J. Phys. G **43**, no.3, 030401 (2016) [arXiv:1507.05613 [physics.ins-det]].